

Vol. 80 Commemorative Accounts

Studies of Organic Protein Cofactors Using Electron Paramagnetic Resonance

Stefan Weber and Robert Bittl*

Freie Universität Berlin, Fachbereich Physik, Institut für Experimentalphysik, Arnimallee 14, 14195 Berlin, Germany

Received August 10, 2007; E-mail: robert.bittl@physik.fu-berlin.de

The elucidation of structural and electronic aspects of paramagnetic organic cofactors in their protein surroundings and related model compounds is a topic of widespread interest. In this field, electron paramagnetic resonance (EPR) spectroscopy, especially in conjunction with high-resolution electron-nuclear double resonance (ENDOR) is an important tool, allowing us to analyze details of the distribution of the unpaired electron spin, which is influenced by the interaction between the cofactor and its immediate environment, as well as to characterize paramagnetic intermediate states in the course of the protein action. In this account, investigations are reported in which EPR/ENDOR methods have contributed significantly to answering questions on mechanistic and structural aspects of protein function. Emphasis is given to in-depth characterizations of electronic and spatial structures of radical cofactors and their positioning relative to substrate molecules. After a brief introduction, covering some of the trends of modern EPR/ENDOR method development, we will focus, as examples, on characterizations of quinone-type and flavin cofactors in two proteins, (i) quinoprotein alcohol dehydrogenase, and (ii) DNA photolyase.

Introduction

Systems containing unpaired electron spins, such as free radicals, biradicals, triplet states, most transition-metal and rare-earth ions, and some point defects in solids form the playground for electron paramagnetic resonance (EPR). In EPR such molecules are studied by observing the magnetic fields, at which they come into resonance with monochromatic continuous-wave or inherently polychromatic pulsed electromagnetic radiation. The fundamentals of EPR are very similar to the more familiar nuclear magnetic resonance (NMR) technique. A number of excellent monographs have appeared in the past covering the basics of EPR.[1–4]

For organic radicals, the main magnetic interaction parameters extracted from EPR spectra are the **g**-matrix and the hyperfine couplings that describe the interaction of the unpaired electron spin with the external magnetic field and the magnetic nuclei in its vicinity, respectively. In some cases, EPR signals are broadened or further split by electron-spin–electron-spin interactions if more than one unpaired electron spin is encountered within a distance of less than 50 to 80 Å. Whereas the isotropic exchange interaction falls off exponentially with the distance between the radicals, the dipolar coupling between the unpaired electron spins decreases with their cubed distance. For not too close radicals (in a weakly coupled radical pair), the exchange interaction is considerably smaller than the dipolar coupling, and the point-dipole approximation may be used to determine the distance between the centers of the unpaired electron spins. For triplet states of organic radicals, on the other hand, the dipolar interaction is orders of magnitudes larger than the hyperfine interactions, and is thus dominating the EPR spectral line shape.

Since its discovery in 1944 by Zavoisky, EPR has typically been performed at frequencies below 40 GHz. This limitation was a technical one, but recent developments in millimeter and sub-millimeter wave and magnet technology have enabled the exploration of ever-growing EPR frequencies. High-magnetic-field/high-microwave-frequency EPR spectroscopy has a number of inherent advantages: (1) The spectral resolution of g-factor differences and anisotropies greatly improves, since the electron-Zeeman interaction scales with the magnetic field. If paramagnetic centers with different g-values or different magnetic sites of rather similar g-values are present, the difference in the spectral magnetic field positions ΔB_0 of the resonances is proportional to the microwave frequency ω

$$\Delta B_0 = \frac{\hbar\omega}{\beta_e}\left(\frac{1}{g_1} - \frac{1}{g_2}\right). \quad (1)$$

In this equation, β_e is the Bohr magneton, and g_1 and g_2 are the g-values of two magnetically different radical species. Even for a single radical, the spectral resolution can be enhanced in disordered solid samples if the inhomogeneous line width is dominated by unresolved hyperfine interactions (HFI). Whereas the hyperfine line broadening $B_{1/2}^{HFI}$ is independent on the magnetic field B_0, the anisotropic **g**-matrix contribution scales linearly with the external magnetic field.

Published on the web December 13, 2007; doi:10.1246/bcsj.80.2270

Thus, if the magnetic field is large enough, i.e., when the condition

$$\frac{\Delta g}{g_{\mathrm{iso}}} B_0 > B_{1/2}^{\mathrm{HFI}}, \tag{2}$$

is fulfilled, the powder spectrum is dominated by the anisotropic **g**-matrix. This equation may be considered as the high-resolution condition for solid-state EPR spectra, to be fulfilled only at high enough magnetic fields B_0. In particular for organic radicals whose g-values are typically very similar to that of the free electron $g_e = 2.0023193$, high magnetic fields are required to resolve the **g**-matrix anisotropy or to unambiguously identify the type of radical involved in a reaction. In the case of well-resolved **g**-anisotropy, the extension to high-field ENDOR has the additional advantage of providing single-crystal-like hyperfine information when transitions are excited at magnetic-field positions, where only specific orientations of **g** with respect of the external magnetic field contribute to the spectrum. (2) Relaxation times become longer for many systems at higher microwave frequencies and magnetic fields. (3) Particularly in studies of small samples, high-magnetic-field/high-microwave-frequency EPR is typically more sensitive as compared to EPR at conventional X-band frequencies (about 9.5 GHz), by virtue of the increased Boltzmann factor and the higher energy of the microwave quanta. Other advantages such as the possibility to detect EPR-silent transitions in high-spin systems using high microwave frequencies or the possibility to violate the high-temperature approximation with standard cryogenic systems are of lesser importance for the characterization of organic radicals and shall not be discussed here.

Disadvantages of high-magnetic-field/high-microwave-frequency EPR are mainly technical ones due to the limited availability of microwave components operating at millimeter or sub-millimeter wavelengths and the high costs of spectrometer development. Nevertheless, these drawbacks are outweighed by the advantages to such an extent that high-magnetic-field/high-microwave-frequency EPR methods will become more and more widespread as one overcomes the technical hurdles. In-depth discussions on the merits of high-field EPR can be found elsewhere.[5–12]

Quinoprotein Alcohol Dehydrogenase

Pyrroloquinoline quinone (PQQ) is one of several quinone derivatives that function as essential cofactors in a class of enzymes known as quinoproteins.[13–15] Special interest in the properties of the PQQ cofactor comes from the fact that its possible role as a vitamin in mammals is currently under debate.[16–19] X-ray crystallographic studies have allowed great progress to be made in the understanding of the structure and function of the PQQ-dependent enzymes.[20–22] The common structural feature of methanol dehydrogenase (MDH) is an $\alpha_2\beta_2$ tetrameric structure,[23–29] in contrast to quinoprotein ethanol dehydrogenase (QEDH), which is a homodimeric protein (α_2).[30,31] In both enzymes, the α-subunit is a superbarrel composed of eight radially arranged β-sheets. The PQQ cofactor forms a complex with a Ca^{2+}-ion buried in the interior of the superbarrel and is sandwiched between the indole ring of a tryptophan and an unusual eight-membered disulfide ring structure formed from adjacent cysteines (see Fig. 1). This

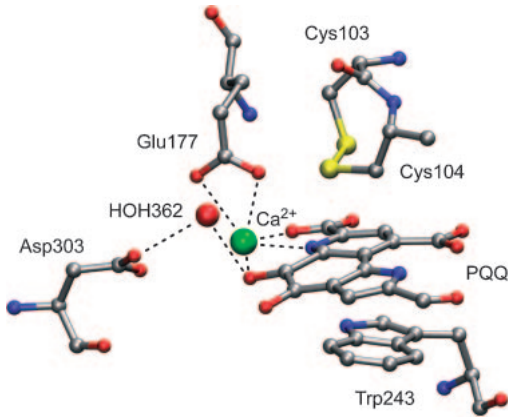

Fig. 1. The active site of methanol dehydrogenase from *Methylobacterium extorquens*.[29] Shown is how the PQQ cofactor bound to Ca^{2+} is sandwiched between Trp243 and the disulfide bridge formed by Cys103 and Cys104. Also shown are the amino-acid residues (Asp303 or Glu177) that have been suggested to play a catalytic role in alcohol oxidation, and a water molecule (HOH362) that forms hydrogen bonds to O(5) of PQQ and Asp303.

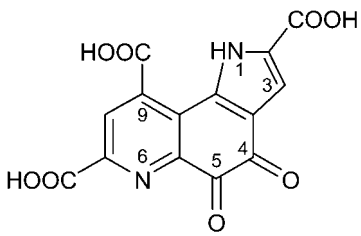

Fig. 2. Molecular structure and IUPAC numbering scheme of the PQQ cofactor.

remarkable ring structure occurs only in PQQ-containing QEDHs. Its function is unknown, although it has been postulated that it could play a role in protecting the intermediate free-radical form of the cofactor.[32] Analysis of the role of this ring structure was the first objective in the investigation of QEDH in our group and is discussed below.

Two alternatives have been proposed for the reaction mechanism in quinoprotein dehydrogenases.[33] Initially, an addition–elimination mechanism was favored, a suggestion that is now considered unlikely,[34] and a hydride-transfer mechanism is preferred.[35] The PQQ is assumed to be initially oxidized, and after substrate binding the reaction is initiated by amino acid–base-catalyzed proton abstraction of the hydroxy proton of the alcohol. The characteristics of an Asp303Glu mutant protein (numbering scheme of MDH from *Methylobacterium extorquens*) were considered consistent with Asp303 acting as the catalytically active base in MDH.[28] Recently, however, this widely accepted view has been challenged with results of a molecular-dynamics study presented by Reddy and Bruice,[36] who suggested that Glu177 is the catalytic base. In either case, nucleophilic addition of the hydride from the substrate to the C(5) position of PQQ is then expected to occur, see Fig. 2. Subsequently, the PQQ enolizes to form the quinol. Reoxidation proceeds in two sequential one-electron transfer steps to cytochrome via the PQQ radical. Establishing the correct protonation state of the PQQ-radical in QEDH, which is a

prerequisite for a proper mechanistic description of the reaction, were the second goal of our EPR/ENDOR experiments.

Oubrie and co-workers have presented a structure of PQQ-dependent soluble glucose dehydrogenase (GDH) in which a complex of reduced PQQ and glucose was resolved at 1.9-Å resolution.[37] The positioning of the C(1)-atom of glucose over the tetrahedral C(5)-atom of PQQ is one of the most convincing pieces of evidence for a hydride-ion transfer mechanism. Thus far, however, a substrate-bound structure for a PQQ-dependent alcohol dehydrogenase has remained elusive. Therefore, we have set out to provide information on substrate binding by EPR and ENDOR spectroscopy.

To characterize the role of the unusual disulfide ring in QEDH, we have applied X- (9.7 GHz) and W-band (94 GHz) continuous-wave EPR spectroscopy on the wild type and a double mutant, Cys105Ala/Cys106Ala, of QEDH.[38] The wild-type as well as the mutant protein were active in a functional assay using an artificial electron acceptor, implying that the disulfide bridge does not play a role in the general mechanism of the enzyme. The X-band continuous-wave EPR spectrum of the PQQ semiquinone radical in the wild-type QEDH enzyme was found to be slightly asymmetric with a line centered at $g_{iso} = 2.0043$, and a peak-to-peak line width of 0.5 mT, which is similar to that observed in GDH,[39] in quinohaemoprotein ethanol dehydrogenase,[40] methylamine dehydrogenase (MADH),[41] and in MDH.[42] A slightly larger peak-to-peak line width of 0.7 mT has been reported for MDH.[15,43] While the resemblance of the PQQ semiquinone spectrum for wild-type QEDH to those of other PQQ-containing dehydrogenases was not unexpected, we surprisingly observed a virtually indistinguishable semiquinone-radical EPR spectrum for the Cys105Ala/Cys106Ala double mutant lacking the disulfide ring that was suggested to stabilize the radical form of the cofactor. The signal intensities of the wild type and the mutant sample were almost identical, indicating a similar radical concentration in both sample types.

In the high-frequency/high-magnetic-field W-band EPR spectra, also no significant difference in the signal intensity between the wild type and the mutant was observed. Previous Q-band (35 GHz) continuous-wave EPR studies yielded an axial **g**-matrix with $g_{\parallel} = 2.0024$ and $g_{\perp} = 2.0056$ for MDH,[15,42] and $g_{\parallel} = 2.0024$ and $g_{\perp} = 2.0048$ for MADH.[41] In the W-band continuous-wave EPR spectra of the QEDH wild type and the double mutant presented in Fig. 3, the full rhombic symmetry of the **g**-matrix is resolved. By spectral simulations, also shown in Fig. 3, including only the principal values of the **g**-matrix and an orientation dependent inhomogeneous EPR line width, reasonable fittings of the experimental data were obtained.

For the wild-type protein, the principal values of the **g**-matrix were determined, $g_X = 2.00575(2)$, $g_Y = 2.00512(2)$, and $g_Z = 2.00209(2)$, yielding $g_{iso} = 2.00432(2)$. X, Y, and Z are the principal axes of **g**. For the double mutant, the principal values of the **g**-matrix are $g_X = 2.00571(2)$, $g_Y = 2.00513(2)$, and $g_Z = 2.00207(2)$, giving $g_{iso} = 2.00430(2)$. The very similar principal values of the wild type and the mutant indicate a virtually identical overall electronic structure of the PQQ semiquinone radical in the both proteins. This finding excludes a particular role of the specific disulfide bridge in QEDH in stabilizing the functional PQQ radical intermediate.

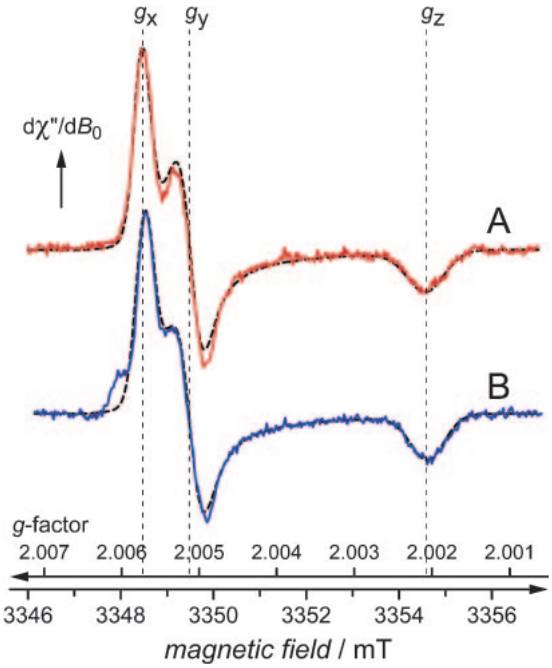

Fig. 3. Continuous-wave W-band EPR spectra of the PQQ cofactor bound in QEDH in the wild type (trace A), and the Cys105Ala/Cys106Ala double mutant (trace B). Also shown are spectral simulations using the **g**-matrix principal values listed in the text. Figure adapted from Ref. 38.

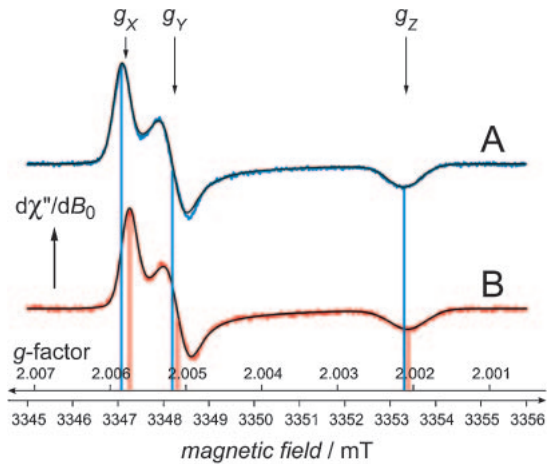

Fig. 4. W-band continuous-wave EPR spectra (blue and red curves) and simulations (black curves) of the PQQ radical bound in wild type QEDH without (trace A), and in the presence of ethanol substrate (trace B). Figure adapted from Ref. 44.

Interestingly, we have found a much more pronounced effect upon presence or absence of the alcohol substrate on the PQQ radical **g**-matrix than on the disulfide bridge,[44] as shown in Fig. 4.

In the substrate-free enzyme, the principal values of the **g**-matrix obtained by spectral simulation are $g_X = 2.00585(2)$, $g_Y = 2.00518(2)$, and $g_Z = 2.00212(2)$, yielding $g_{iso} = 2.00438(2)$. All three principal values of the **g**-matrix decrease when the substrate ethanol is bound to the enzyme,

$g_X = 2.00574(2)$, $g_Y = 2.00511(2)$, and $g_Z = 2.00207(2)$, yielding $g_{iso} = 2.00431(2)$. The observed changes were completely reversible. Either spectrum could be generated sequentially from the same sample (or from different protein preparations) by removal or addition of the ethanol substrate. These differences between the g-values represented the first spectral evidence for tight binding of ethanol to the PQQ–Ca^{2+} complex in alcohol dehydrogenases. The shifts in the **g**-matrix components of the radical are likely to be a consequence of a changed environment and/or geometry of the PQQ cofactor. From work on nitroxide spin labels,[45] para-semiquinones,[46,47] and tyrosyl radicals,[48] it is well-known that the g_X component of compounds with a high spin density on a carbonyl or NO group is particularly sensitive to changes in its immediate vicinity. In the case of PQQ in QEDH, all three components became smaller in the presence of ethanol, although the g_X component shows the biggest shift of about 1×10^{-4}, see Fig. 4. A binding motif for the substrate obtained from ENDOR studies is consistent with this high-field EPR result and will be discussed below. Before that, however, we turn to the analysis of the protonation state of the PQQ radical in QEDH by ENDOR techniques.[49] X-band pulsed ENDOR spectra of the PQQ radical bound in QEDH and reconstituted in protiated and deuteriated buffer were recorded and are displayed in panels A and B of Fig. 5, respectively.

The ENDOR spectra are centered at the nuclear Zeeman frequency ($\nu_H = 14.75$ MHz), and in the weak-coupling limit, which is the case here, each set of equivalent protons gives rise to a pair of tensorial patterns, whereby the splitting is equal to the hyperfine coupling component (Fig. 5, traces A and B). To aid comparison, the spectra have been normalized such that the outer shoulder and peak in the range of $\nu_H \pm 6$–10 MHz, which appear to be almost unaffected by changes in the buffer, have the same intensity. The spectrum from QEDH reconstituted in protiated buffer (trace A of Fig. 5) exhibits a very rich and well-resolved hyperfine structure with couplings in the range from 0 to 10 MHz. When the enzyme was reconstituted in deuteriated buffer (trace B of Fig. 5), there was a dramatic reduction in intensity in the middle part of the spectrum. The difference between the spectra recorded in deuteriated buffer and protiated buffer is shown as trace C of Fig. 5. The difference spectrum gives us a high degree of confidence that the solvent-exchangeable protons have hyperfine couplings in the range between 0 and 5 MHz. One of these exchangeable protons is expected to be that attached to N(1). The protonation states of the three carboxylic acid groups of PQQ, when bound in quinoproteins, are not known, although in solution at pH 7 it is expected that they would be deprotonated.[39,50] Nevertheless, even if they were protonated, such protons always have negligible hyperfine couplings. The only other positions in the cofactor that could have exchangeable protons with significant hyperfine couplings are at O(4) and O(5). Other contributions can arise from exchangeable protons of water molecules in the binding pocket, or of nearby amino acids such as the arginine at position 344, see Fig. 1.

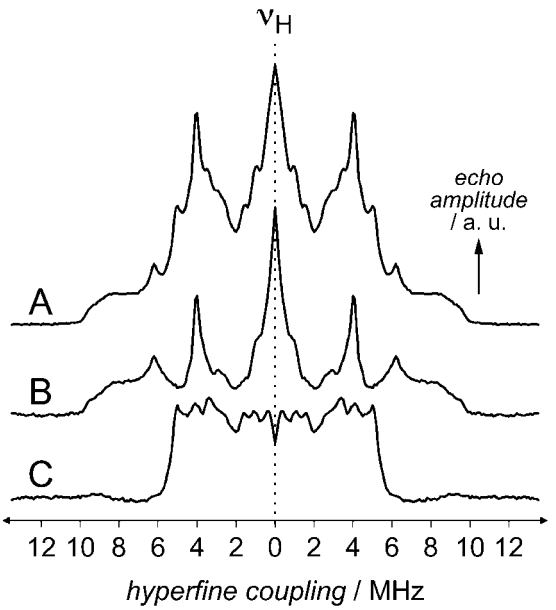

Fig. 5. Pulsed X-band ENDOR spectra of the PQQ radical bound in wild-type QEDH. The enzyme was reconstituted in H_2O buffer (trace A) and in D_2O buffer (trace B). Trace C shows the difference between traces A and B.[49] Figure adapted from Ref. 49.

The spectrum from the sample reconstituted in deuteriated buffer (Fig. 5, trace B) should contain only non-exchangeable protons, of which the PQQ cofactor has two, one at C(3) and the other at C(8). Indeed, outside of the matrix region (hyperfine couplings larger than 2 MHz), two tensorial patterns can be identified. One has rhombic symmetry as is expected for an α-proton with components at 9.6 and 6.2 MHz, whereas the third and smallest component is smaller and overlaps with other resonances. The second has a narrow and intense component at 4.0 MHz, which implies unexpected axial symmetry, although the other component cannot be positively identified.

The matrix region (hyperfine couplings smaller than 2 MHz) shows an intense signal and some structure, but it cannot be easily interpreted. These couplings are probably in part due to the β-protons on the cysteine residues forming a disulfide bridge that is in van der Waals contact with the PQQ cofactor.

To gain a more complete understanding of the spectrum containing only the non-exchangeable protons, pulsed ENDOR experiments have been performed at W-band. The improved spectral resolution provided by the increased Zeeman interaction allows us to measure ENDOR spectra with orientation selection from non-oriented frozen protein samples. In Fig. 6, the X-band ENDOR spectrum (trace A) is shown in comparison with the W-band spectra (traces B, C, and D) of the same sample, recorded at magnetic-field positions in the W-band EPR spectrum at which principal values of the **g**-matrix are on resonance (see Figs. 3 and 4).

Comparison of the X-band (trace A) and W-band ENDOR (traces B to D) spectra clearly demonstrates the advantage of high-frequency ENDOR. The powder-type ENDOR spectrum obtained at X-band frequency is separated into three more simple spectra at W-band. The most straightforward ENDOR spectrum to interpret is that with the magnetic field parallel to the Z-axis of **g** (Fig. 6, trace D). Given that the π-plane of the PQQ cofactor is approximately planar, an assumption that all X-ray data and quantum-mechanical calculations support, then (as in all quinoids) Z is expected to be perpendicular

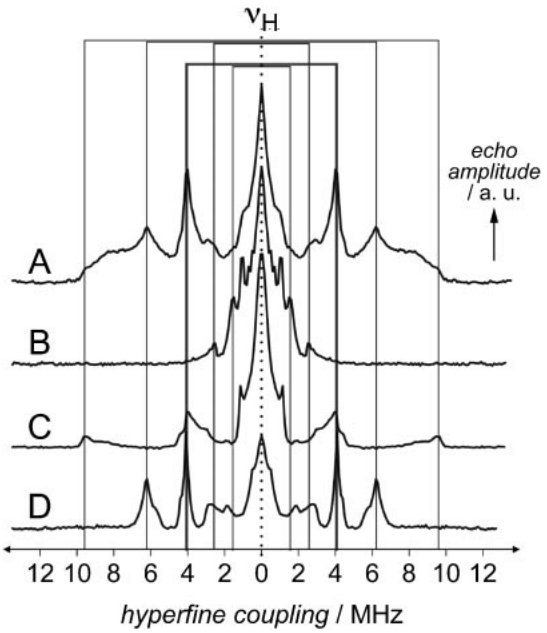

Fig. 6. Pulsed ENDOR spectra of the PQQ radical bound in wild-type QEDH reconstituted in D_2O buffer at X-band (trace A) and at W-band (traces B, C, and D). The W-band ENDOR spectra were recorded at magnetic-field positions corresponding to molecules with their **g** principal axes parallel to the external magnetic field, i.e., $B_0 \parallel X$ (trace B), $B_0 \parallel Y$ (trace C), and $B_0 \parallel Z$ (trace D). Also shown are two pairs of three lines corresponding to the three principal components of the two hyperfine tensors discussed in the text. Figure adapted from Ref. 49.

to the molecular frame. Hence, only molecules with their planes perpendicular to the external magnetic field are on resonance at this position. Therefore, only the component of the hyperfine coupling tensor that is perpendicular to the molecular plane is detected. For the α-protons at C(3) and C(8) of PQQ, see Fig. 2, this is the middle hyperfine coupling component, and indeed, the spectrum recorded at g_Z shows two intense transitions, with A_Z couplings of 6.2 and 4.0 MHz. These are also observed at X-band (see trace A of Fig. 6).

The spectrum recorded at g_Y (Fig. 6, trace C) also shows two distinct, albeit broader transitions: a large hyperfine coupling with a maximum at 9.6 MHz and a smaller one of 4.1 MHz. Again, these can be associated directly with the equivalent transitions in the X-band ENDOR spectrum. Finally, in the spectrum taken at g_X (Fig. 6, trace B), all large hyperfine couplings have vanished and only a single pair of lines with a coupling of 2.6 MHz is observed outside the intense matrix region. On the flanks of the matrix region is another pair of lines with a splitting of 1.6 MHz. Compiling all this information, one symmetric rhombic tensor with components $A_X = 2.6$ MHz, $A_Y = 9.6$ MHz, and $A_Z = 6.2$ MHz, and one almost axial tensor with components $A_X = 1.6$ MHz, $A_Y = 4.1$ MHz, and $A_Z = 4.0$ MHz can be assigned to the two non-exchangeable protons.

The interpretation of the observed ENDOR spectra has been based on density-functional theory (DFT) calculations comparing three different assumed protonation states of the PQQ radical.[49] Only the hyperfine couplings calculated for the unprotonated form of $PQQ^{\bullet}$ complexed to Ca^{2+} (formally $PQQ^{4-\bullet}Ca^{2+}$) have been found in agreement with the experimentally obtained values. This agreement led to a model for the singly occupied molecular orbital (SOMO) of the radical species that has highest electron densities at O(4), C(5), and O(5) on the central ring. This result is a beautiful example of the theory of orbital steering,[51] as this orbital in its guises as SOMO (in the radical form) and lowest-unoccupied molecular orbital (LUMO) (in the oxidized form) has optimal spatial form to function in twin roles, as acceptor for a hydride transfer from the substrate and as electron donor with good overlap with the orbitals of the disulfide bridge, thus promoting electron transfer to cytochrome and reoxidation of the PQQ. Hence, these results obtained by ENDOR spectroscopy in conjunction with DFT calculations support the proposed hydride-transfer mechanism and an electron-transfer pathway via the disulfide bridge. For the reduced PQQ, energetics and the character of the highest-occupied molecular orbital (HOMO) clearly indicate that O(5) is deprotonated. As a consequence it was suggested that reduced PQQ is singly protonated at O(4), although a doubly deprotonated species cannot be entirely excluded.[49]

Although the EPR spectrum of the PQQ radical bound in MDH was first observed many years ago,[15] its nature has only been correctly determined by ENDOR,[49] thus ending the unfortunate situation where the wrong structure has been used as a basis for mechanistic discussions. The actual structure of the PQQ radical bound in a quinoprotein and the suggestion for the structure of the reduced PQQ species provide the basis for a corrected reaction scheme in which electron- and proton-transfer pathways may be examined meaningfully.

As a last example for EPR/ENDOR on the PPQ radical in QEDH we discuss a model for substrate binding obtained from ENDOR spectroscopy using the substrate analogue ethanol.[52] ENDOR spectra recorded at X-band in the presence or absence of methanol are highly similar, but show very well reproducible subtle differences as shown in Fig. 7.

The differences between the methanol-bound and methanol-free samples are indicated by arrows. The well-resolved hyperfine coupling components of the larger of the two α-proton hyperfine coupling tensors of the PQQ radical decrease upon methanol binding while the two components of the smaller proton hyperfine coupling tensor increase. These changes in the hyperfine couplings upon binding of methanol corroborate the conclusion from the high-field EPR experiments (see above),[44] that the substrate comes in close contact with the PQQ radical. As in the case of the high-field EPR spectra, the spectral shifts in the ENDOR spectra upon binding or removal of substrate have been found to be completely reversible. The close proximity between the PQQ radical and the substrate has been demonstrated even more clearly by differences between ENDOR spectra taken with unlabeled (CH_3OH) and isotope-labeled (CD_3OH) methanol. The difference spectrum shows an axial hyperfine pattern due to the methyl group of methanol.[52] The observed hyperfine coupling is consistent with a distance between the substrate and the PQQ radical of only about 3 Å.

To interpret the observed changes in the PQQ hyperfine

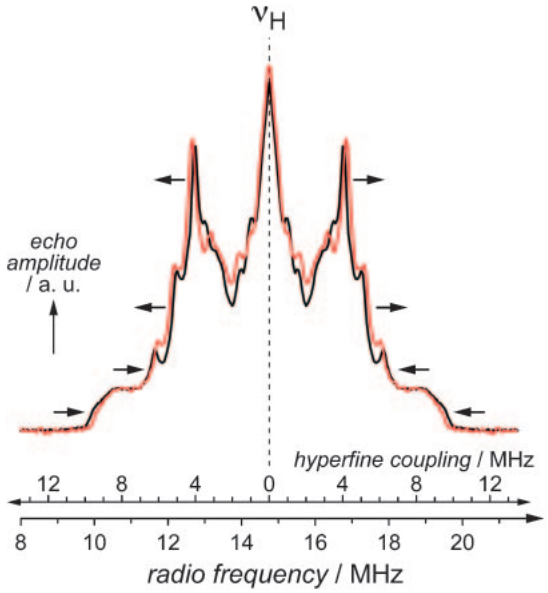

Fig. 7. Pulsed X-band ENDOR spectra of the PQQ radical bound in wild-type QEDH. Shown are spectra substrate-free (black line) and with methanol substrate bound (red line). Arrows indicate the hyperfine couplings that become either larger or smaller in the presence of methanol. Figure adapted from Ref. 52.

structure in terms of a binding geometry of the substrate, again DFT calculations have been performed.[52] The qualitative and quantitative differences in the hyperfine couplings could only be reproduced by calculations under the assumption of a binding model where the substrate replaces a water molecule found in the X-ray structure of MDH.[29] This binding motif invokes an involvement of a conserved Asp residue and is consistent with findings from a mutagenesis study.[28] The binding motif is also consistent with the changes in the **g**-matrix components as observed by high-field EPR,[44] although the alterations of **g** are not as specific to the binding motif as are the hyperfine couplings. An alternative binding model involving instead a glutamic acid residue, suggested on the basis of a molecular-dynamics study,[36] resulted in changes in the hyperfine couplings which are in qualitative disagreement with the experimental observations. The ENDOR-based binding motif put forward by us,[52] has recently been questioned by a new molecular-dynamics study by Zhang and co-workers.[53] However, the treatment of the Ca^{2+}-ion bound to the PQQ cofactor remains unclear in the description of their procedures.[53] Proper inclusion of Ca^{2+} has been found to be of critical importance in the DFT calculation of the PQQ hyperfine couplings. Thus, differences in the computational approaches are very likely the origin for the discrepancy of the molecular-dynamics results,[36,53] and the conclusions based on ENDOR data.[52]

Photolyases

Ultraviolet (UV) radiation in the 100–320 nm spectral region has carcinogenic, mutagenic, and fatal effects on living organisms.[54] The most significant cellular target of UV is DNA. When DNA is exposed to radiation at wavelengths approaching its absorption maximum at around 260 nm, adjacent pyrimidines within the same DNA strand may become covalently linked by the formation of mainly (70–80%) four-membered ring structures referred to as cyclobutane pyrimidine dimers (CPDs) and also (20–30%) of pyrimidine (6–4) pyrimidone photoproducts ((6–4)PPs),[54] see Fig. 8. Exact yields and the type of damage depend on the sequence and structure, the curvature and the folding of DNA.

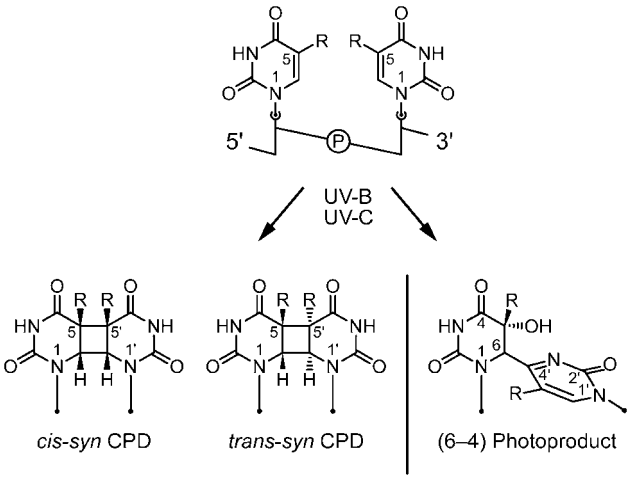

Fig. 8. The structures of the most frequently encountered mutagenic DNA lesions induced by UV light. R denotes either H in uracil or CH_3 in thymine. The *cis–syn* CPD is a diastereoisomer of the *trans–syn* CPD.

Photoreactivation by photolyase uses UV-A (320–400 nm) and blue light (400–500 nm) to monomerize pyrimidine dimers in DNA.[55–73] Photolyases have been reported in many vertebrates including reptiles, fish, and marsupials. Apart from some transgenic mice[74] it seems that placental mammals are generally devoid of DNA photolyases.[75–77]

All photolyases described to date are monomeric proteins with molecular masses in the 45 to 66 kD range.[55] Photolyases are distinguished by their substrate specificity: DNA photolyase (also called CPD photolyase) binds and repairs CPD lesions, whereas (6–4) photolyase acts upon (6–4)PP-damages. DNA photolyases are further classified into class-I and class-II, depending on their amino-acid sequence similarity.[78–80] Class-I photolyases are found in many bacteria and archaea, but in eukaryotes, they are found only in fungi. Class-II photolyases are the most divergent group of the family and are additionally present in plants,[81–85] green algae,[86] dipterans,[87] and vertebrates.[88] All known photolyases contain stoichiometric amounts of non-covalently bound flavin adenine dinucleotide (FAD) as redox-active cofactor.[78,82,85,87,89–95] The enzymatic activity of photolyases depends on the photoexcited state of FAD in the fully reduced form, $FADH^-$, see Fig. 9, whereas the vast majority of other flavoproteins utilize the ground state[96–98] or the excited state of the fully oxidized redox state of flavin, FAD^{ox}.

$FADH^-$ in photolyases has weak absorbance at wavelengths below and vanishing absorbance above 400 nm. A second (also non-covalently bound) chromophore is also often present and functions as a light-harvesting cofactor to increase the absorption cross-section of the enzyme and to extend its absorbance to longer wavelengths. According to the type of light-harvesting cofactor present, either a folate (5,10-methenyltetrahydro-

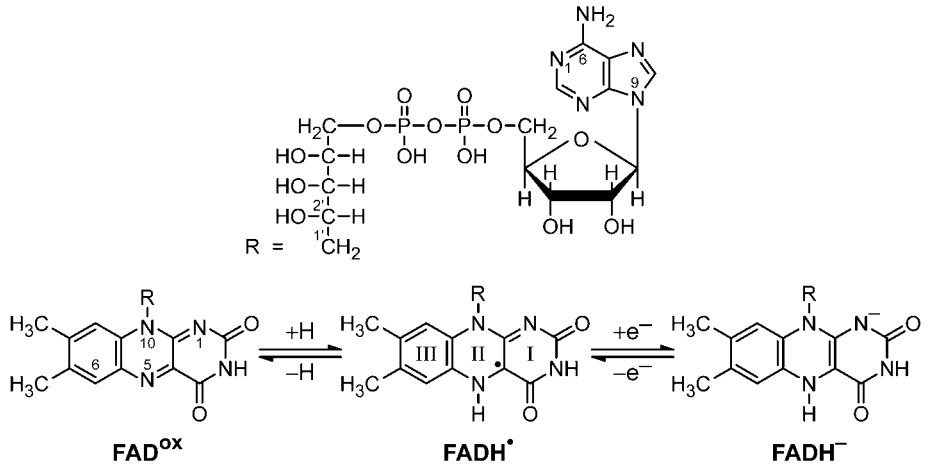

Fig. 9. The biologically relevant redox states of flavin adenine dinucleotide. The IUPAC numbering scheme is shown for FAD^{ox}.

folylpolyglutamate (MTHF)) or a deazaflavin (8-hydroxy-5-deazaflavin (8-HDF)), class-I photolyase are further categorized into either MTHF-type or 8-HDF-type. (6–4) photolyases also contain FAD as redox-active cofactor.[94,99] They have been found in *D. melanogaster*,[100–102] *Xenopus laevis* (South African clawed toad),[94,103] *Crotalus atrox* (rattlesnake),[103] *Danio rerio* (zebrafish),[104] *A. thaliana*,[83,105,106] and the marine hexactinellid sponge *Aphrocallistes vastus*.[107]

In a seminal contribution by Park and co-workers, the three-dimensional structure of the class-I DNA photolyase from *E. coli* was determined by X-ray crystallography at 2.3 Å resolution.[108] Subsequently, the crystal structures of the (class-I) 8-HDF-type DNA photolyase and apo-photolyase from *A. nidulans* were elucidated, both at 1.8 Å resolution.[109,110] The *E. coli* and *A. nidulans* enzymes show similar backbone structures of their respective single polypeptide chain, consistent with the conserved function and the very homologous amino-acid sequences. The FAD cofactor is bound to a helical domain. An α/β-domain provides binding sites for the respective second chromophore. Both the location and conformation of the redox-active FAD are virtually identical in all structurally characterized photolyases. The molecule is bent in a unique U-shaped configuration so that the adenine ring comes in close contact with the 7,8-dimethyl isoalloxazine ring. In all three enzymes, the flavin cofactor is buried in the center of the helical domain with solvent access limited to a cavity leading from the surface to the edge of the adenine moiety of FAD. A band of positive electrostatic potential, suitable for contact with the negatively charged phosphate backbone of the damaged DNA strand, runs along the outside of the protein around the cavity entrance. One side of the cavity consists of hydrophobic amino-acid residues, and the other side has polar groups. This asymmetry is also a property of the CPD site of damaged DNA, in which the cyclobutane ring is hydrophobic and the opposite edges of the thymine bases have nitrogens and oxygens capable of forming hydrogen bonds. The cavity opening is wide enough to accommodate a CPD provided that it is extruded from the duplex.[108] Such base-flipping out of double-helical DNA has been observed in many DNA-repair systems, in which the enzymes need to approach the DNA bases in order to perform a reaction on them.[111]

Two types of photoreaction have been observed in photolyases: (i) photorepair of UV-damaged DNA by the catalytically active enzyme with its FAD cofactor in the fully reduced redox state, $FADH^-$, and (ii) photoactivation of the catalytically inert enzyme. The latter reaction takes place when the FAD cofactor is in a redox state different from $FADH^-$, i.e., FAD semiquinone, $FADH^\bullet$, or fully oxidized FAD^{ox} (see Fig. 9). The commonly accepted model for the individual steps of the enzymatic repair reaction in CPD-splitting DNA photolyase and the (6–4) photoproduct-repairing (6–4) photolyase is summarized in Fig. 10. The experimental data that led to the proposition of radical mechanisms for the repair reactions of the DNA photodamages is summarized in recent review articles.[72,73,112] Nevertheless, one should keep in mind that important details in the catalytic pathway have not yet been conclusively established and therefore require further examination.

In the above-mentioned photoreactions of photolyases, the paramagnetic semiquinone form, $FADH^\bullet$, plays an important role as a reaction intermediate or as reactant, respectively. The fact that the FAD cofactor in most photolyases is easily oxidized into its semiquinone form during enzyme isolation and purification in an aerobic environment thus makes EPR and ENDOR ideally suited to specifically study this functional intermediate state without having to discriminate the signal from a background in a mixture of redox states because $FADH^-$ and FAD^{ox} are both diamagnetic. In-depth EPR characterizations of $FADH^\bullet$ are prerequisite for the quantitative analysis of time-resolved EPR spectra from short-lived radical-pair states, that have been generated by photoexcitation of photolyase with the flavin in the fully oxidized redox state.[73,113,114]

A stationary continuous-wave EPR signal in DNA photolyase was first reported by Jorns and co-workers. Given its line width of 1.9 mT, the signal was attributed to a neutral (N(5)-protonated) flavin signal.[91] Subsequently, the same signal centered at around $g = 2.0038$ has been published by several groups, although no further interpretation of the line width and the emerging hyperfine structure was given.[113,115–118] By EPR at W-band (94 GHz) we have determined the principal values of the **g**-tensors of $FADH^\bullet$ in DNA photolyase and (6–4) photolyase, although due to the incomplete resolution of the anisotropic Zeeman interaction at these microwave frequencies, some uncertainties in the g_X, g_Y, and g_Z values

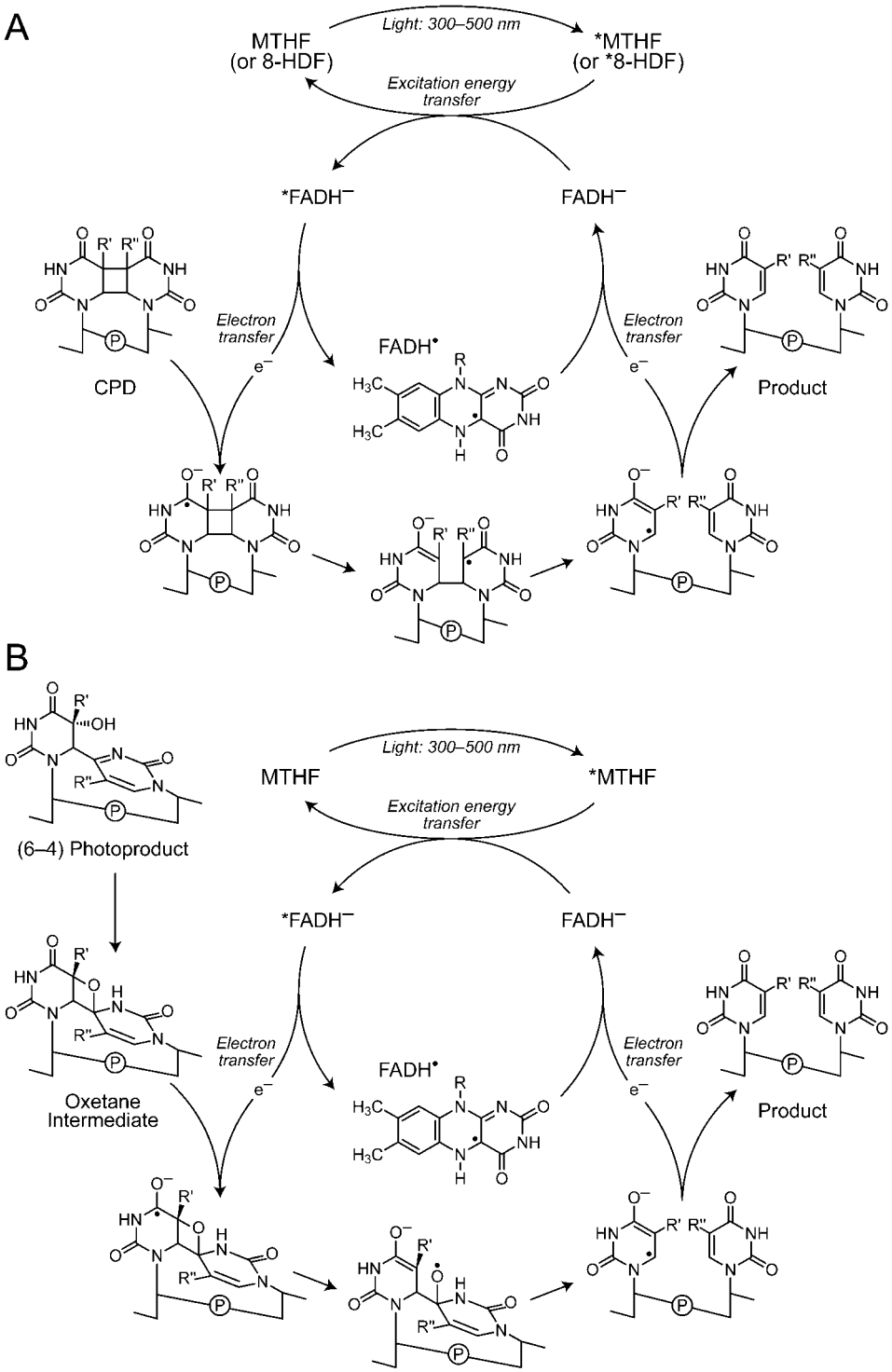

Fig. 10. The putative reaction mechanism of CPDs by DNA photolyase (A) and (6–4) photoproducts by (6–4) photolyase (B). R is defined in Fig. 9. R′ and R″ are either CH_3 in thymine or H in uracil.

remained.[119,120] Only at very high microwave frequencies and correspondingly high magnetic fields, 360 GHz and 12.8 T, respectively, the stable radical EPR signal of photolyases can be fully resolved, i.e., the high-field condition is fulfilled, so that the **g**-matrix anisotropy is exposed, see Fig. 11.[121,122] By least-squares fittings of spectral simulations to experimental data, the principal values of the **g**-matrix of FADH• from *E. coli* DNA photolyase and *X. laevis* (6–4) photolyase have been established: $g_X = 2.00431(5)$, $g_Y = 2.00360(5)$, $g_Z = 2.00217(7)$ for DNA photolyase, and $g_X = 2.00433(5)$, $g_Y = 2.00368(5)$, $g_Z = 2.00218(7)$ for (6–4) photolyase.

Comparing the g-values given above for FADH• bound to DNA photolyase and the identical cofactor molecule bound to (6–4) photolyase, a difference in the g_Y-value can be ascertained while the g_X- and g_Z-values are the same within experimental error, see Fig. 11. It is expected that this shift is

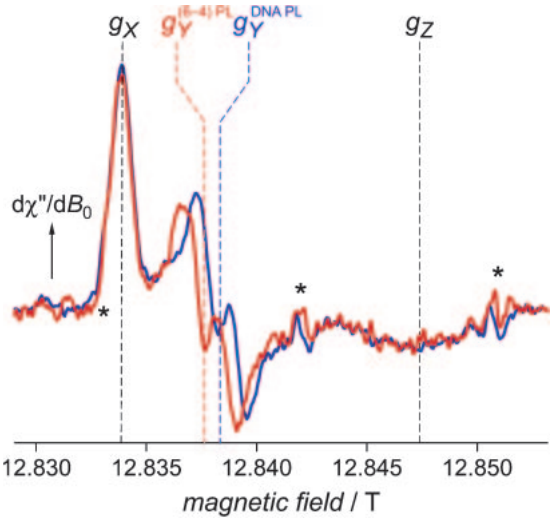

Fig. 11. 360.03-GHz continuous-wave EPR spectra of the neutral flavin semiquinone cofactors FADH• in the DNA photolyase of *E. coli* (blue curve),[121] and the (6–4) photolyase of *X. laevis* (red curve).[122] The spectra have been recorded at $T = 200$ K. The asterisks indicate regions that contain small artifacts due to the Mn^{II}/MgO magnetic-field standard lines. Figure adapted from Ref. 122.

induced by changes in the electron-spin density distribution on the flavin moiety. These may be either caused by modulations of the cofactor-binding pocket, in particular through hydrogen bonds between the cofactor and the protein, or by a deviation of the electronic π-system from planarity. An amino-acid alignment of *E. coli* DNA photolyase and *X. laevis* (6–4) photolyase reveals that the flavin-binding pocket is highly conserved with the exception of one amino-acid residue in the primary coordination sphere. In DNA photolyase, an alanine residue (Ala377 in *E. coli*) is situated above the pyrimidine ring of the flavin and close to both carbonyl bonds, C(2)=O(2) and C(4)=O(4). Molecular modeling has shown that in (6–4) photolyase (no crystal structure is available to date) the alanine residue is replaced by leucine with its more bulky $-CH_2-CH(CH_3)_2$ tail pointing toward the C(2)=O(2) direction. Although in the *E. coli* DNA photolyase X-ray structural analysis no water molecules have been detected in this region,[108] if present, they would be clearly displaced in the (6–4) photolyase by the leucine residue, thus altering the local polarity. That in flavin radicals the g_Y component proves to be more sensitive than g_X and g_Z towards local changes in the electronic environment is most probably due to the different symmetries of the isoalloxazine moiety of the flavin as compared for example with nitroxides, quinones, and tyrosines, where usually the g_X principal component is more responsive.[45–48] The latter molecules have a well-defined symmetry axis with X aligned either along the N–O or C=O bonds, respectively, and there is a high unpaired electron-spin density on the oxygens. Hence, they are particularly sensitive to changes in the hydrogen-bonding situation in this direction. Flavins, on the other hand, have much lower symmetry, with the two carbonyl groups being meta-positioned, see Fig. 9. Furthermore, the unpaired electron-spin density is more localized on C(4a) and N(5) rather than on the carbonyl groups where the oxygens

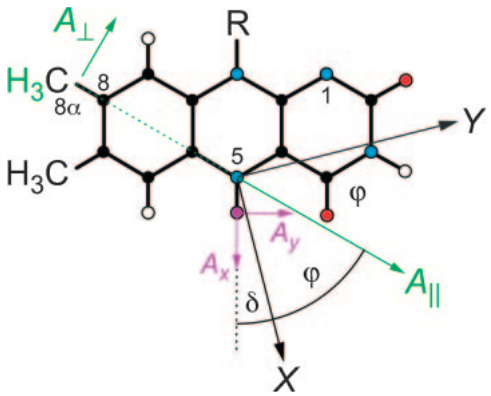

Fig. 12. 7,8-Dimethyl isoalloxazine moiety of FADH•. R denotes the ribityl side chain. φ represents the angle between the $A_\parallel$ component of the hyperfine coupling tensor of H(8α) and the X axis of **g**, and δ is the angle between the N(5)–H bond (this is parallel to the x axis of the hyperfine tensor of H(5)) and the X axis of **g**. The Z axis is oriented perpendicular to the molecular plane of FADH•. The principal axes of the hyperfine tensors of H(8α) and H(5) are drawn in green and magenta, respectively.

have only a very small share of the total unpaired electron spin.[123] Clearly, such studies demonstrate, that the **g**-matrix reflects local changes in the protein–cofactor interaction, but very high magnetic fields are required to resolve these subtle changes. They remain unobserved due to the large inhomogeneous broadening from unresolved hyperfine interactions in EPR at conventional microwave-frequency bands.

To unambiguously determine the **g**-matrix orientation with respect to the molecular coordinate system of a radical, usually quite labor-extensive single-crystal studies have to be performed. Fortunately, in the case of neutral flavin radicals one can forgo these costly and time-consuming experiments and determine the orientation of the principal axes from a splitting of the g_Y resonance observed in the 360-GHz/12.8-T EPR spectra, see Fig. 11.[121,122] This splitting is due to the hyperfine coupling of the strongly coupled α-proton H(5), the assignment being based on 360-GHz EPR studies on deuterium-exchanged FADH• in DNA photolyase.[121] The anisotropic hyperfine coupling constant of H(5) was obtained by proton-ENDOR, which revealed the principal values $A_x = (-)8.5$ MHz,[124] $A_y = (-)37.0$ MHz, $A_z = (-)24.9$ MHz for *E. coli* DNA photolyase,[125] and $A_x = (-)13.7$ MHz, $A_y = (-)38.4$ MHz, $A_z = (-)26.1$ MHz for *X. laevis* (6–4) photolyase.[120] x, y, and z are the principal axes of the hyperfine tensor of H(5) and are aligned along the N–H-bond, perpendicular the N–H bond in the π-plane of the isoalloxazine ring, and perpendicular to the π-plane, respectively, see Fig. 12. Assuming that the Z principal axis of **g** coincides with the plane normal of the isoalloxazine moiety, then the rotation angle $|\delta|$ between the Y axis of **g** and the y axis of the H(5) hyperfine coupling tensor is obtained by relating A_Y to A_y, see Fig. 12.[121] Since the observed hyperfine splitting of $(-)36.4$ MHz (in the case of *E. coli* DNA photolyase) at the g_Y-edge is almost as large as the largest principal value of the H(5) hyperfine tensor ($A_y = (-)37.0$ MHz, see above), the **g**-axis corresponding to the principal value g_Y, i.e., the Y-axis, must be oriented

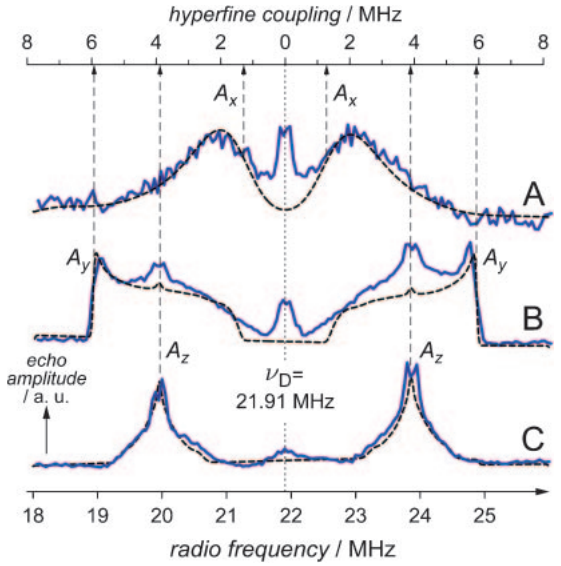

Fig. 13. W-band pulsed deuterium ENDOR spectra of the flavin cofactor of *E. coli* DNA photolyase in deuteriated buffer (solid blue curves) recorded at different magnetic-field positions in the EPR spectrum: (A) $B_0 \parallel g_X$, (B) $B_0 \parallel g_Y$, and (C) $B_0 \parallel g_X$. Figure adapted from Ref. 125.

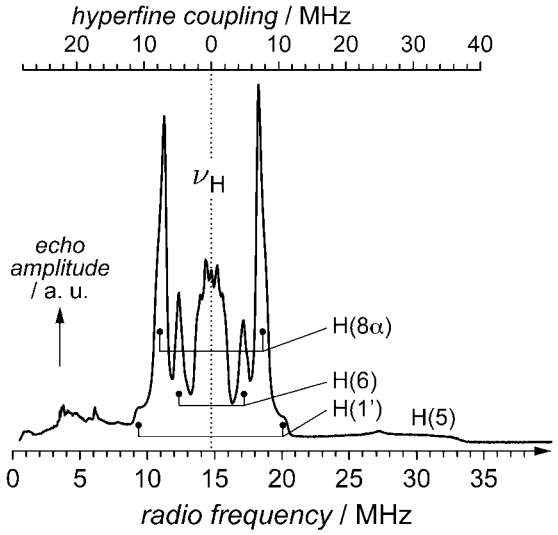

Fig. 14. X-band pulsed (Davies) ENDOR spectrum of the neutral flavin semiquinone cofactor FADH• of *E. coli* DNA photolyase. Figure adapted from Ref. 125.

roughly parallel to the molecular *y*-axis.[121] The small deviation of the splitting at g_Y from the A_y-value determined by ENDOR must then be due to the tilt angle of the molecule-fixed hyperfine tensor principal axes with respect to those of the **g**-tensor. The remaining ambiguity in the sign of the tilt angle can be removed by comparing the orientation of **g** with respect to a second hyperfine tensor, e.g., the one from the methyl protons H(8α), which then returns only one consistent geometric solution.[126] Again, the orientation selection of high-field ENDOR has been prerequisite for a precise determination of the angle δ, which has been found to be $-14 \pm 2^\circ$ for FADH• from *E. coli* DNA photolyase,[126] and $-29 \pm 4^\circ$ for *X. laevis* (6–4) photolyase.[120] This demonstrates nicely that also the orientation of the principal axes of **g** changes noticeably upon alterations of the cofactor surroundings.

Interestingly, scaling the anisotropic proton hyperfine coupling components of H(5) by multiplication with the quotient of the magnetogyric ratio of a deuteron and a proton, $\gamma_D/\gamma_H = 1/6.5144 = 0.15351$, and comparing these "scaled" values with those of the respective deuteron couplings that were directly measured by W-band deuterium ENDOR spectroscopy on an H → D buffer-exchanged sample, see Fig. 13, reveals subtle but reproducible differences. A direct measurement of the D(5) hyperfine coupling and its anisotropy by ENDOR is only possible at very high magnetic fields by exploiting the orientation selection near the high-field limit, because at lower fields the deuteron resonances strongly overlap with those from nitrogens and protons. At W-band frequencies, however, the resonance range of the deuterons is well separated from those of other types of nuclei. The differences between the scaled proton hyperfine couplings and the deuteron hyperfine couplings can be attributed to the different lengths of the N(5)–H(5) and N(5)–D(5) bonds from the different masses of protons and deuterons. From the r^{-3}-dependence of the dipolar hyperfine splitting, it can be estimated that the N(5)–D bond is about 2.5% shorter than the respective N(5)–H bond in *E. coli* DNA photolyase. Hence, the anisotropy of the hyperfine tensors of H(5) or D(5) bound to N(5) in the isoalloxazine moiety of flavins appears to be a sensitive probe of the bond length. As the bond length is also influenced by the hydrogen-bond strength to neighboring amino acids, this opens up a novel method to probe hydrogen bonding in flavoproteins with the flavin cofactor in the neutral radical form. As information on the hydrogen-bond strength is difficult to extract from the crystal structure of a flavoprotein in general (due to the typically restricted spatial resolution), pulsed ENDOR spectroscopy, by exploiting the orientation selection at high magnetic fields on non-oriented samples, provides a valuable tool for the studies of protein–cofactor interactions in flavoproteins.[125]

The hyperfine interactions arising from other protons attached to the 7,8-dimethyl isoalloxazine moiety of the FAD cofactor as obtained from proton ENDOR spectroscopy can also be exploited to probe the immediate environment of the flavin, in particular hydrogen bonding and the micropolarity. Two prominent features are typically observed in the ENDOR spectra of flavin neutral radicals, see Fig. 14. The tensorial line shapes with hyperfine couplings at around 6.5–8 MHz are of almost axial symmetry and arise from the hyperfine couplings of the β-protons H(8α) of the methyl group attached to C(8). Typically, methyl groups rotate about their C–C bond at elevated temperatures. Hence, if this rotation is fast on the ENDOR time scale, one common hyperfine tensor for all three protons of the methyl group is observed. Signals of the H(8α) hyperfine tensor are in general easily detected in proton-ENDOR spectroscopy on flavins, and are considered to be sensitive probes of the electron-spin density on the xylene ring (ring III, see Fig. 9) of the flavin isoalloxazine moiety. Furthermore, theory shows that the size of this coupling responds sensitively to polarity changes of the protein surroundings.[127] The isotropic hyperfine couplings of the H(8α) methyl protons but also the one of the H(6) proton in photolyases are among the smallest values reported for neutral flavin semiquinones of flavoproteins so far. Therefore, the unpaired electron spin

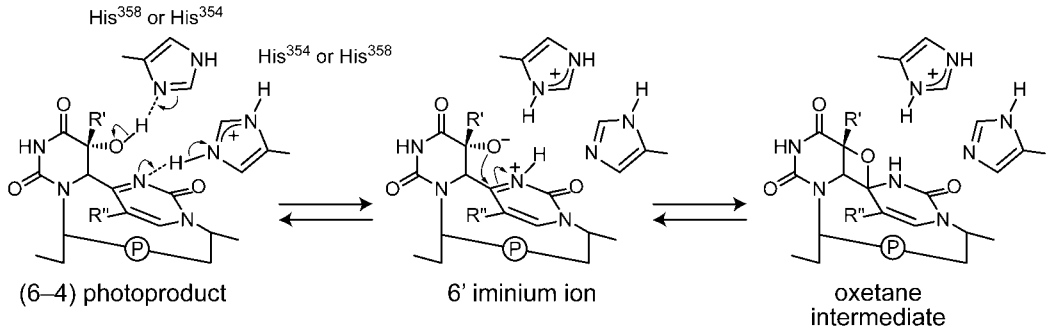

Fig. 15. The proposed mechanism for oxetane intermediate formation in *X. laevis* (6–4) photolyase. R′ and R″ are either CH_3 in thymine or H in uracil.

density must be significantly shifted to the central pyrazine ring (ring II, see Fig. 9) and the pyrimidine ring (ring I, see Fig. 9) of the isoalloxazine moiety. One possible reason for this peculiarity might be the specific location of the FAD cofactor in the protein: The pyrimidine part of the isoalloxazine ring is directed toward the interior of the enzyme: in particular it is covered by polar amino acids, such as Asp372 and Arg344 in *E. coli* DNA photolyase, that bind the flavin through hydrogens bonds. The xylene part of FAD at the opposite side, however, points toward the putative substrate binding pocket, and, driven by its hydrophobicity, facilitates the docking of the enzyme to the CPD in the DNA substrate. The absence of any stabilizing aromatic amino-acid residues, such as tyrosines or tryptophans, near this part of the flavin, therefore, does not promote distribution of the unpaired spin over the entire isoalloxazine moiety. This might have some interesting functional implications: Once an electron is transferred from the reduced flavin, $FADH^-$, to the CPD, and a transient $FADH^\bullet$ radical is formed, the rather poor stabilization of the unpaired electron spin over the isoalloxazine moiety might favor back-transfer of the electron from the then repaired CPD to the flavin. In an unpolar environment, backward electron transfer might be pushed into the Marcus inverted region of electron transfer, thus increasing the efficiency of the CPD cleavage reaction. To what extent the unique U-shaped conformation of the FAD in photolyases, as determined from X-ray crystallography,[108] plays an important part in the spin density distribution remains to be clarified.

That the H(8α) proton hyperfine coupling of the $FADH^\bullet$ radical in (6–4) photolyase is even smaller than that of *E. coli* DNA photolyase,[128] implies an even less polar and/or more aromatic environment of this enzyme, which might be due to one or both of the following changes relative to the *E. coli* enzyme: (i) a smaller substrate-binding pocket for (6–4) photoproducts in (6–4) photolyase that would limit the number of water molecules that could approach the redox-active flavin cofactor in the absence of a DNA lesion; and (ii) two aromatic histidine residues, His354 and His358, that are predicted to replace non-aromatic Asn and Met in *E. coli* photolyase render the cofactor binding site more aromatic. These histidines play a role in catalyzing the formation of an oxetane intermediate from the (6–4) photoproduct that precedes light-initiated DNA repair, see Fig. 15.[129] Unlike DNA photolyases, (6–4) photolyases are not able to directly restore the original bases from the (6–4) photoproduct in UV-damaged DNA. Rather, following binding of the lesion, the overall repair reaction consists of two distinct steps, one of which is light-independent and the other one light-dependent, see Fig. 10, panel B. In the initial light-independent step, a 6′-iminium ion is thought to be generated via proton transfer induced by the two abovementioned histidines in *X. laevis* photolyase, that are highly conserved among the (6–4) photolyases in general. This intermediate spontaneously rearranges to form an oxetane intermediate by intramolecular nucleophilic attack. Such a mechanism requires that one histidine acts as a proton acceptor and the other as a proton donor, Fig. 15, which implies that the two histidines should have markedly different pK_a values.

Data from pulsed (Davies) proton ENDOR spectroscopy provided the first experimental evidence that this model is essentially correct, see Fig. 16.[128] The hyperfine splittings of the H(8α) and H($1'$) protons shifted significantly as a function of structural modifications induced by point mutations and pH changes. In the absence of an X-ray structure for a (6–4) photolyase, we proposed that His354 is close to H($1'$) of the $FADH^\bullet$, and His358 is close to the H(8α) methyl protons. Furthermore, the data is consistent with His358 being deprotonated at pH 9 where the (6–4) photoproduct repair activity is highest. His354 is likely to be protonated and thus is the histidine residue that initiates formation of the oxetane intermediate from the (6–4) photoproduct, Fig. 15, in the enzymatic DNA repair reaction.

As a final example to demonstrate the potential of EPR and ENDOR in probing the docking of substrate molecules to enzymes, we present data from *E. coli* DNA photolyase bound to a CPD-containing DNA substrate, see Fig. 17. The $FADH^\bullet$ in its neutral radical form served us here as a naturally occurring spin probe.[127] Small shifts of the proton hyperfine couplings of the flavin were observed when UV-damaged DNA was bound to the enzyme in comparison to substrate-free enzyme, see Fig. 17. The changes of the hyperfine couplings upon binding of substrate are very small and imply a lower limit of about 6 Å for the distance between the CPD and the location of maximum unpaired electron-spin density in the flavin's isoalloxazine ring. In a separate contribution, using DFT calculations, we have shown that the orbital in which the unpaired electron spin is located has maximum density on the C(4a) and N(5) atoms.[123] Hence, the 6-Å distance estimated from ENDOR should be applied from this position rather than from the C(8α) methyl group. The observed subtle shifts of the isotropic proton hyperfine-coupling constants of the isoalloxazine

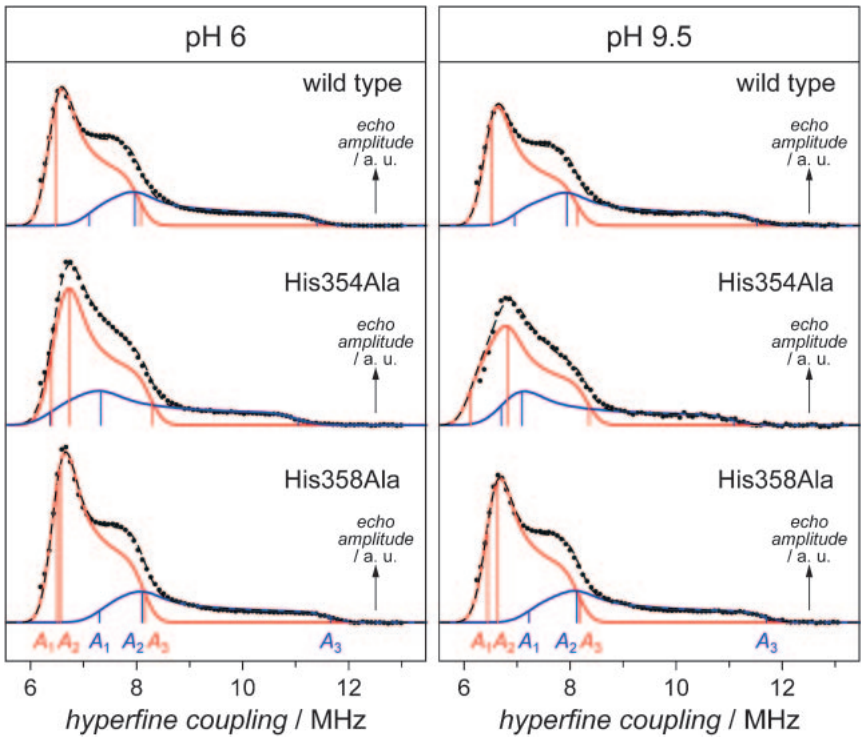

Fig. 16. X-band pulsed (Davies) ENDOR spectra of FADH• bound to wild-type and mutant *X. laevis* (6–4) photolyase at different pH values. Only the high radio-frequency region with the H(8α) and H(1′) resonances is shown. The red and blue curves show the contributions of the H(8α) and H(1′) hyperfine couplings to the overall calculated (dashed black curves) and experimental ENDOR spectra, respectively. The vertical lines show the positions of the principal hyperfine components of the hyperfine tensors. Figure adapted from Ref. 128.

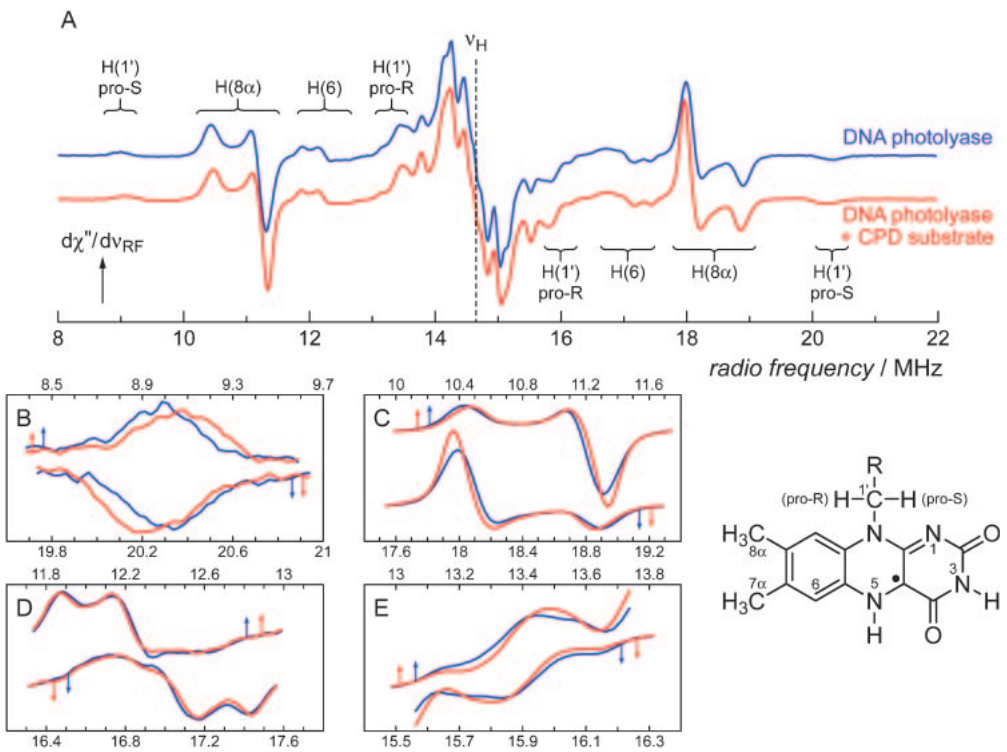

Fig. 17. X-band continuous-wave ENDOR frozen-solution spectra of the neutral flavin radical FADH• in DNA photolyase from *E. coli* without (A, upper curve in blue) and with (A, lower curve in red) bound CPD substrate recorded at 160 K. The panels B to E show enlargements of various radio-frequency ranges of the spectra of panel A. The arrows indicate the radiofrequency axes to which the spectral traces belong. Figure adapted from Ref. 127.

moiety have been rationalized in terms of changing polarity of the cofactor environment once the substrate is docked to the enzyme. The trends observed are consistent with the substrate-binding pocket becoming less polar because of the displacement of water molecules upon substrate binding.[127]

Very recently, the long-awaited X-ray crystal structure of *A. nidulans* DNA photolyase bound to a CPD-like DNA lesion was presented by Mees and co-workers,[130] finally showing that the CPD lesion is indeed flipped out of the DNA helix into the active site of the enzyme. The separation between the CPD-like DNA lesion and the flavin cofactor is closer than commonly expected.[131,132] With a distance of about 4.3 Å between the C(8) methyl group of the isoalloxazine moiety of FAD and the 3′-thymine, and about 7 Å between the center of the electron-donating $FADH^-$ ring to the CPD-like lesion, the prediction from ENDOR was in a reasonably good agreement. A direct electron-transfer pathway for CPD repair cannot be excluded at such a relatively close distance between the CPD and the redox-active flavin cofactor. From the co-crystal structure, however, it appears likely that the flavin's adenine moiety is involved in forward and back electron transfer.

Concluding Remarks

In this review, we have used the examples of the paramagnetic quinone and flavin cofactors in QEDH and various photolyases to discuss the potential of EPR and ENDOR spectroscopy for structural and functional investigations of protein complexes. Thereby, we have stressed in particular the importance and the advantages of a multi-frequency approach, combining the strengths of classical X-band (9 GHz) with those of modern high-field/high-frequency EPR up to 360 GHz. A second important aspect in recent EPR applications is the interpretation of the experimental data by DFT-type electronic-structure calculations. The results of such EPR/ENDOR studies often provide the molecular basis for a proper mechanistic description of protein function not available on the basis of protein structure data alone.

We are grateful to all co-workers involved in the studies discussed here, in particular Dr. Chris Kay (now: University College London), and Dr. Erik Schleicher. We gratefully acknowledge our long-term collaboration partners Professor Adelbert Bacher (Technische Universität München), Professor Elizabeth Getzoff and Dr. Kenichi Hitomi (Scripps Research Institute), Professor Helmut Görisch (Technische Universität Berlin), Professor Peter Hegemann (Humboldt-Universität zu Berlin), Professor Klaus Möbius (Freie Universität Berlin), Professor Gerald Richter (Cardiff University), and Professor Takeshi Todo (Osaka University). This work was supported by Deutsche Forschungsgemeinschaft (Sfb-498 TP A2 and C5).

References

1 C. P. Keijzers, E. J. Reijerse, J. Schmidt, *Pulsed EPR: A New Field of Applications*, North Holland, Amsterdam, The Netherlands, **1989**.

2 N. M. Atherton, *Principles of Electron Spin Resonance*, Ellis Horwood Limited, Chichester, West Sussex, PO19 1EB, England, **1993**.

3 J. A. Weil, J. R. Bolton, J. E. Wertz, *Electron Paramagnetic Resonance. Elementary Theory and Practical Applications*, John Wiley & Sons, Inc., New York, NY, **1994**.

4 A. Schweiger, G. Jeschke, *Principles of Pulse Electron Paramagnetic Resonance*, Oxford University Press, Oxford, **2001**.

5 D. Goldfarb, *Phys. Chem. Chem. Phys.* **2006**, *8*, 2325.

6 K. Möbius, A. Savitsky, A. Schnegg, M. Plato, M. Fuchs, *Phys. Chem. Chem. Phys.* **2005**, *7*, 19.

7 M. Bennati, T. F. Prisner, *Rep. Prog. Phys.* **2005**, *68*, 411.

8 G. Jeschke, *Biochim. Biophys. Acta* **2005**, *1707*, 91.

9 O. Grinberg, L. J. Berliner, *Very High Frequency (VHF) ESR/EPR*, Kluwer Academic/Plenum Publishers, New York, **2004**.

10 S. Un, P. Dorlet, A. W. Rutherford, *Appl. Magn. Reson.* **2001**, *21*, 341.

11 K. Möbius, *Chem. Soc. Rev.* **2000**, *29*, 129.

12 J. H. Freed, *Annu. Rev. Phys. Chem.* **2000**, *51*, 655.

13 J. G. Hauge, *J. Biol. Chem.* **1964**, *239*, 3630.

14 C. Anthony, L. J. Zatman, *Biochem. J.* **1967**, *104*, 960.

15 J. A. Duine, J. Frank, J. Westerling, *Biochim. Biophys. Acta* **1978**, *524*, 277.

16 T. Kasahara, T. Kato, *Nature* **2003**, *422*, 832.

17 L. M. Felton, C. Anthony, *Nature* **2005**, *433*, E10.

18 R. Rucker, D. Storms, A. Sheets, E. Tchaparian, A. Fascetti, *Nature* **2005**, *433*, E10.

19 T. Kasahara, T. Kato, *Nature* **2005**, *433*, E11.

20 C. Anthony, *Biochem. J.* **1996**, *320*, 697.

21 J. A. Duine, *J. Biosci. Bioeng.* **1999**, *88*, 231.

22 C. Anthony, *Arch. Biochem. Biophys.* **2004**, *428*, 2.

23 C. C. F. Blake, M. Ghosh, K. Harlos, A. Avezoux, C. Anthony, *Nat. Struct. Biol.* **1994**, *1*, 102.

24 M. Ghosh, C. Anthony, K. Harlos, M. G. Goodwin, C. Blake, *Structure* **1995**, *3*, 177.

25 Z.-x. Xia, W.-w. Dai, Y.-f. Zhang, S. A. White, G. D. Boyd, F. S. Mathews, *J. Mol. Biol.* **1996**, *259*, 480.

26 Z.-x. Xia, Y.-n. He, W.-w. Dai, S. A. White, G. D. Boyd, F. S. Mathews, *Biochemistry* **1999**, *38*, 1214.

27 Y.-J. Zheng, Z.-x. Xia, Z.-w. Chen, F. S. Mathews, T. C. Bruice, *Proc. Natl. Acad. Sci. U.S.A.* **2001**, *98*, 432.

28 P. R. Afolabi, F. Mohammed, K. Amaratunga, O. Majekodunmi, S. L. Dales, R. Gill, D. Thompson, J. B. Cooper, S. P. Wood, P. M. Goodwin, C. Anthony, *Biochemistry* **2001**, *40*, 9799.

29 P. A. Williams, L. Coates, F. Mohammed, R. Gill, P. T. Erskine, A. Coker, S. P. Wood, C. Anthony, J. B. Cooper, *Acta Crystallogr., Sect. D: Biol. Crystallogr.* **2005**, *61*, 75.

30 A. Diehl, F. v. Wintzingerode, H. Görisch, *Eur. J. Biochem.* **1998**, *257*, 409.

31 T. Keitel, A. Diehl, T. Knaute, J. J. Stezowski, W. Höhne, H. Görisch, *J. Mol. Biol.* **2000**, *297*, 961.

32 A. Avezoux, M. G. Goodwin, C. Anthony, *Biochem. J.* **1995**, *307*, 735.

33 C. Anthony, P. Williams, *Biochim. Biophys. Acta* **2003**, *1647*, 18.

34 A. Oubrie, B. W. Dijkstra, *Protein Sci.* **2000**, *9*, 1265.

35 C. Anthony, M. Ghosh, C. C. Blake, *Biochem. J.* **1994**, *304*, 665.

36 S. Y. Reddy, T. C. Bruice, *J. Am. Chem. Soc.* **2003**, *125*, 8141.

37 A. Oubrie, H. J. Rozeboom, K. H. Kalk, A. J. J. Olsthoorn, J. A. Duine, B. W. Dijkstra, *EMBO J.* **1999**, *18*, 5187.

38 C. W. M. Kay, B. Mennenga, H. Görisch, R. Bittl, *FEBS*

Lett. **2004**, *564*, 69.
39 A. Sato, K. Takagi, K. Kano, N. Kato, J. A. Duine, T. Ikeda, *Biochem. J.* **2001**, *357*, 893.
40 G. A. H. De Jong, A. Geerlof, J. Stoorvogel, J. A. Jongejan, S. De Vries, J. A. Duine, *Eur. J. Biochem.* **1995**, *230*, 899.
41 R. de Beer, J. A. Duine, J. Frank, P. J. Large, *Biochim. Biophys. Acta* **1980**, *622*, 370.
42 R. de Beer, D. van Ormondt, M. A. van Ast, R. Banen, J. A. Duine, J. Frank, *J. Chem. Phys.* **1979**, *70*, 4491.
43 J. Westerling, J. Frank, J. A. Duine, *Biochem. Biophys. Res. Commun.* **1979**, *87*, 719.
44 C. W. M. Kay, B. Mennenga, H. Görisch, R. Bittl, *J. Am. Chem. Soc.* **2005**, *127*, 7974.
45 T. Kawamura, S. Matsunami, T. Yonezawa, *Bull. Chem. Soc. Jpn.* **1967**, *40*, 1111.
46 O. Burghaus, M. Plato, M. Rohrer, K. Möbius, F. MacMillan, W. Lubitz, *J. Phys. Chem.* **1993**, *97*, 7639.
47 R. A. Isaacson, F. Lendzian, E. C. Abresch, W. Lubitz, G. Feher, *Biophys. J.* **1995**, *69*, 311.
48 S. Un, M. Atta, M. Fontecave, A. W. Rutherford, *J. Am. Chem. Soc.* **1995**, *117*, 10713.
49 C. W. M. Kay, B. Mennenga, H. Görisch, R. Bittl, *J. Biol. Chem.* **2006**, *281*, 1470.
50 K. Kano, K. Mori, B. Uno, T. Kubota, T. Ikeda, M. Senda, *Bioelectrochem. Bioenerg.* **1990**, *24*, 193.
51 A. D. Mesecar, B. L. Stoddard, D. E. Koshland, Jr., *Science* **1997**, *277*, 202.
52 C. W. M. Kay, B. Mennenga, H. Görisch, R. Bittl, *Proc. Natl. Acad. Sci. U.S.A.* **2006**, *103*, 5267.
53 X. Zhang, S. Y. Reddy, T. C. Bruice, *Proc. Natl. Acad. Sci. U.S.A.* **2007**, *104*, 745.
54 E. C. Friedberg, G. C. Walker, W. Siede, *DNA Repair and Mutagenesis*, ASM Press, Washington, D.C., **1995**.
55 G. B. Sancar, *Mutat. Res.* **1990**, *236*, 147.
56 A. Sancar, in *Advances in Electron Transfer Chemistry*, ed. by P. E. Mariano, JAI Press, London, **1992**, Vol. 2, p. 215.
57 P. F. Heelis, S.-T. Kim, T. Okamura, A. Sancar, *J. Photochem. Photobiol., B* **1993**, *17*, 219.
58 S.-T. Kim, A. Sancar, *Photochem. Photobiol.* **1993**, *57*, 895.
59 A. Sancar, *Biochemistry* **1994**, *33*, 2.
60 P. F. Heelis, R. F. Hartman, S. D. Rose, *Chem. Soc. Rev.* **1995**, *24*, 289.
61 T. Carell, *Angew. Chem., Int. Ed. Engl.* **1995**, *34*, 2491.
62 P. F. Heelis, R. F. Hartman, S. D. Rose, *J. Photochem. Photobiol., A* **1996**, *95*, 89.
63 A. Sancar, *Science* **1996**, *272*, 48.
64 X. Zhao, D. Mu, *Histol. Histopathol.* **1998**, *13*, 1179.
65 F. Thoma, *EMBO J.* **1999**, *18*, 6585.
66 T. Todo, *Mutat. Res.* **1999**, *434*, 89.
67 G. B. Sancar, *Mutat. Res.* **2000**, *451*, 25.
68 J. Deisenhofer, *Mutat. Res.* **2000**, *460*, 143.
69 T. Carell, L. T. Burgdorf, L. M. Kundu, M. Cichon, *Curr. Opin. Chem. Biol.* **2001**, *5*, 491.
70 R. P. Sinha, D.-P. Häder, *Photochem. Photobiol. Sci.* **2002**, *1*, 225.
71 C. L. Thompson, A. Sancar, *Oncogene* **2002**, *21*, 9043.
72 A. Sancar, *Chem. Rev.* **2003**, *103*, 2203.
73 S. Weber, *Biochim. Biophys. Acta* **2005**, *1707*, 1.
74 W. Schul, J. Jans, Y. M. A. Rijksen, K. H. M. Klemann, A. P. M. Eker, J. de Wit, O. Nikaido, S. Nakajima, A. Yasui, J. H. J. Hoeijmakers, G. T. J. van der Horst, *EMBO J.* **2002**, *21*, 4719.
75 C. C.-K. Chao, *FEBS Lett.* **1993**, *336*, 411.
76 Y. F. Li, S.-T. Kim, A. Sancar, *Proc. Natl. Acad. Sci. U.S.A.* **1993**, *90*, 4389.
77 R. D. Ley, *Proc. Natl. Acad. Sci. U.S.A.* **1993**, *90*, 4337.
78 A. Yasui, A. P. M. Eker, S. Yasuhira, H. Yajima, T. Kobayashi, M. Takao, A. Oikawa, *EMBO J.* **1994**, *13*, 6143.
79 S. Kanai, R. Kikuno, H. Toh, H. Ryo, T. Todo, *J. Mol. Evol.* **1997**, *45*, 535.
80 K. Hitomi, K. Okamoto, H. Daiyasu, H. Miyashita, S. Iwai, H. Toh, M. Ishiura, T. Todo, *Nucleic Acids Res.* **2000**, *28*, 2353.
81 M. Ahmad, J. A. Jarillo, L. J. Klimczak, L. G. Landry, T. Peng, R. L. Last, A. R. Cashmore, *Plant Cell* **1997**, *9*, 199.
82 O. Kleiner, J. Butenandt, T. Carell, A. Batschauer, *Eur. J. Biochem.* **1999**, *264*, 161.
83 C.-Z. Jiang, J. Yee, D. L. Mitchell, A. B. Britt, *Proc. Natl. Acad. Sci. U.S.A.* **1997**, *94*, 7441.
84 S. Takahashi, N. Nakajima, H. Saji, N. Kondo, *Plant Cell Physiol.* **2002**, *43*, 342.
85 T. Hirouchi, S. Nakajima, T. Najrana, M. Tanaka, T. Matsunaga, J. Hidema, M. Teranishi, T. Fujino, T. Kumagai, K. Yamamoto, *Mol. Genet. Genomics* **2003**, *269*, 508.
86 J. L. Petersen, D. W. Lang, G. D. Small, *Plant Mol. Biol.* **1999**, *40*, 1063.
87 S.-T. Kim, K. Malhotra, H. Ryo, A. Sancar, T. Todo, *Mutat. Res.* **1996**, *363*, 97.
88 T. Kato, Jr., T. Todo, H. Ayaki, K. Ishizaki, T. Morita, S. Mitra, M. Ikenaga, *Nucleic Acids Res.* **1994**, *22*, 4119.
89 N. Iwatsuki, C. O. Joe, H. Werbin, *Biochemistry* **1980**, *19*, 1172.
90 A. Sancar, G. B. Sancar, *J. Mol. Biol.* **1984**, *172*, 223.
91 M. S. Jorns, G. B. Sancar, A. Sancar, *Biochemistry* **1984**, *23*, 2673.
92 A. P. M. Eker, P. Kooiman, J. K. C. Hessels, A. Yasui, *J. Biol. Chem.* **1990**, *265*, 8009.
93 A. P. M. Eker, H. Yajima, A. Yasui, *Photochem. Photobiol.* **1994**, *60*, 125.
94 T. Todo, S.-T. Kim, K. Hitomi, E. Otoshi, T. Inui, H. Morioka, H. Kobayashi, E. Ohtsuka, H. Toh, M. Ikenaga, *Nucleic Acids Res.* **1997**, *25*, 764.
95 R. Kato, K. Hasegawa, Y. Hidaka, S. Kuramitsu, T. Hoshino, *J. Bacteriol.* **1997**, *179*, 6499.
96 V. Massey, *FASEB J.* **1995**, *9*, 473.
97 M. W. Fraaije, A. Mattevi, *Trends Biochem. Sci.* **2000**, *25*, 126.
98 C. W. M. Kay, S. Weber, in *Electron Paramagnetic Resonance*, ed. by B. C. Gilbert, M. J. Davies, D. M. Murphy, Royal Society of Chemistry, Cambridge, UK, **2002**, Vol. 18, p. 222.
99 K. Hitomi, S.-T. Kim, S. Iwai, N. Harima, E. Otoshi, M. Ikenaga, T. Todo, *J. Biol. Chem.* **1997**, *272*, 32591.
100 T. Todo, H. Takemori, H. Ryo, M. Ihara, T. Matsunaga, O. Nikaido, K. Sato, T. Nomura, *Nature* **1993**, *361*, 371.
101 S.-T. Kim, K. Malhotra, C. A. Smith, J.-S. Taylor, A. Sancar, *J. Biol. Chem.* **1994**, *269*, 8535.
102 T. Todo, H. Ryo, K. Yamamoto, H. Toh, T. Inui, H. Ayaki, T. Nomura, M. Ikenaga, *Science* **1996**, *272*, 109.
103 S.-T. Kim, K. Malhotra, J.-S. Taylor, A. Sancar, *Photochem. Photobiol.* **1996**, *63*, 292.
104 Y. Kobayashi, T. Ishikawa, J. Hirayama, H. Daiyasu, S. Kanai, H. Toh, I. Fukuda, T. Tsujimura, N. Terada, Y. Kamei, S. Yuba, S. Iwai, T. Todo, *Genes Cells* **2000**, *5*, 725.
105 J.-J. Chen, D. L. Mitchell, A. B. Britt, *Plant Cell* **1994**,

6, 1311.
106 S. Nakajima, M. Sugiyama, S. Iwai, K. Hitomi, E. Otoshi, S.-T. Kim, C.-Z. Jiang, T. Todo, A. B. Britt, K. Yamamoto, *Nucleic Acids Res.* **1998**, *26*, 638.
107 H. C. Schröder, A. Krasko, D. Gundacker, S. P. Leys, I. M. Müller, W. E. G. Müller, *Biochim. Biophys. Acta* **2003**, *1651*, 41.
108 H.-W. Park, S.-T. Kim, A. Sancar, J. Deisenhofer, *Science* **1995**, *268*, 1866.
109 T. Tamada, K. Kitadokoro, Y. Higuchi, K. Inaka, A. Yasui, P. E. de Ruiter, A. P. M. Eker, K. Miki, *Nat. Struct. Biol.* **1997**, *4*, 887.
110 R. Kort, H. Komori, S.-i. Adachi, K. Miki, A. P. M. Eker, *Acta Crystallogr., Sect. D: Biol. Crystallogr.* **2004**, *60*, 1205.
111 R. J. Roberts, X. Cheng, *Annu. Rev. Biochem.* **1998**, *67*, 181.
112 L.-O. Essen, T. Klar, *Cell Mol. Life Sci.* **2006**, *63*, 1266.
113 Y. M. Gindt, E. Vollenbroek, K. Westphal, H. Sackett, A. Sancar, G. T. Babcock, *Biochemistry* **1999**, *38*, 3857.
114 S. Weber, C. W. M. Kay, H. Mögling, K. Möbius, K. Hitomi, T. Todo, *Proc. Natl. Acad. Sci. U.S.A.* **2002**, *99*, 1319.
115 S.-T. Kim, A. Sancar, C. Essenmacher, G. T. Babcock, *J. Am. Chem. Soc.* **1992**, *114*, 4442.
116 C. Essenmacher, S.-T. Kim, M. Atamian, G. T. Babcock, A. Sancar, *J. Am. Chem. Soc.* **1993**, *115*, 1602.
117 S. Kim, A. Sancar, C. Essenmacher, G. T. Babcock, *Proc. Natl. Acad. Sci. U.S.A.* **1993**, *90*, 8023.
118 R. R. Rustandi, M. S. Jorns, *Biochemistry* **1995**, *34*, 2284.
119 C. W. M. Kay, R. Feicht, K. Schulz, P. Sadewater, A. Sancar, A. Bacher, K. Möbius, G. Richter, S. Weber, *Biochemistry* **1999**, *38*, 16740.
120 C. W. M. Kay, E. Schleicher, K. Hitomi, T. Todo, R. Bittl, S. Weber, *Magn. Reson. Chem.* **2005**, *43*, S96.
121 M. Fuchs, E. Schleicher, A. Schnegg, C. W. M. Kay, J. T. Törring, R. Bittl, A. Bacher, G. Richter, K. Möbius, S. Weber, *J. Phys. Chem. B* **2002**, *106*, 8885.
122 A. Schnegg, C. W. M. Kay, E. Schleicher, K. Hitomi, T. Todo, K. Möbius, S. Weber, *Mol. Phys.* **2006**, *104*, 1627.
123 S. Weber, K. Möbius, G. Richter, C. W. M. Kay, *J. Am. Chem. Soc.* **2001**, *123*, 3790.
124 The parenthesis indicate that the sign of the hyperfine coupling constant have not been determined experimentally and were taken from quantum-chemical computations.
125 S. Weber, C. W. M. Kay, A. Bacher, G. Richter, R. Bittl, *ChemPhysChem* **2005**, *6*, 292.
126 C. W. M. Kay, R. Bittl, A. Bacher, G. Richter, S. Weber, *J. Am. Chem. Soc.* **2005**, *127*, 10780.
127 S. Weber, G. Richter, E. Schleicher, A. Bacher, K. Möbius, C. W. M. Kay, *Biophys. J.* **2001**, *81*, 1195.
128 E. Schleicher, K. Hitomi, C. W. M. Kay, E. D. Getzoff, T. Todo, S. Weber, *J. Biol. Chem.* **2007**, *282*, 4738.
129 K. Hitomi, H. Nakamura, S.-T. Kim, T. Mizukoshi, T. Ishikawa, S. Iwai, T. Todo, *J. Biol. Chem.* **2001**, *276*, 10103.
130 A. Mees, T. Klar, P. Gnau, U. Hennecke, A. P. M. Eker, T. Carell, L.-O. Essen, *Science* **2004**, *306*, 1789.
131 D. B. Sanders, O. Wiest, *J. Am. Chem. Soc.* **1999**, *121*, 5127.
132 J. Hahn, M.-E. Michel-Beyerle, N. Rösch, *J. Phys. Chem. B* **1999**, *103*, 2001.

Stefan Weber was born in 1963, studied chemistry in Stuttgart, and received his diploma and Dr. rer. nat. at the Institute of Physical Chemistry of the University of Stuttgart with Prof. Dr. Gerd Kothe. Thereafter, he received a Feodor-Lynen fellowship of the Alexander-von-Humboldt foundation to carry out postdoctoral research from 1995–1997 with Prof. James R. Norris at the Chemistry Department of the University of Chicago. In 1997 he moved to Berlin and in 2003 received his habilitation in Experimental Physics at the Freie Universität (FU) Berlin. He is a senior scientist at the Physics Department of the FU and also manages the Collaborative Research Center 498 "Protein-Cofactor Interactions in Biological Processes" of the Deutsche Forschungsgemeinschaft. His current research interests include the application of advanced magnetic-resonance techniques to paramagnetic intermediates in photoactive proteins.

Robert Bittl was born in 1959, studied physics in Munich, and received his diploma and doctoral degree at the Department of Physics of the Technische Universität München with Prof. Klaus Schulten. After postdoctoral research from 1989–1991 at the Universität Stuttgart with Prof. Dr. Gerd Kothe he joined the group of Prof. Dr. Wolfgang Lubitz at the Chemistry Department of Technische Universität Berlin where he obtained his habilitation in Physical Chemistry in 1997. Since 2001 he is Professor for Experimental Physics at the Freie Universität Berlin where he is also chairman of the Collaborative Research Center 498 "Protein-Cofactor Interactions in Biological Processes" of the Deutsche Forschungsgemeinschaft. His current research interests are electron paramagnetic resonance and fluorescence single-molecule spectroscopy.